Circular dichroism of single-wall carbon nanotubes

Naomichi Sato, Yuki Tatsumi, and Riichiro Saito
Department of Physics, Tohoku University, Sendai 980-8578, Japan
(Received 27 November 2016; revised manuscript received 13 March 2017; published 21 April 2017)

Circular dichroism (CD) of a single-wall carbon nanotube (SWNT) is calculated as a function of the wavelength of light. Because of the symmetry between the K and K' points in the hexagonal Brillouin zone, the conventional theory for CD intensity gives a zero value in which the absorption probability near the K point for right-handed circular polarized light and that near the K' point for left-handed circular polarized light cancel each other. Considering the phase differences of the light for carbon atoms of a nanotube, which are beyond so-called dipole approximation, a formulation of CD for a SWNT is presented. Analytic and numerical calculations show (1) the alternating sign of the CD intensity at E_{ii} ($i = 1,2,3,\ldots$) van Hove singular energies and (2) opposite sign of the CD values as a function of wavelength of the light for different types and handedness of nanotubes, which reproduce the experimental results. In the metallic SWNTs, we predict the opposite sign of CD values for split E_{ii}^{+} and E_{ii}^{-}.

DOI: 10.1103/PhysRevB.95.155436

I. INTRODUCTION

The circular dichroism (CD) of a material is defined by a difference of optical absorption for left-handed circular polarized light (LCP) and right-handed circular polarized light (RCP). Nonzero CD values as a function of the wavelength of light are observed for materials that have an enantiomer, where an enantiomer is the mirror image of a molecule (solid) that is not superposable to the original molecule (solid). Separation and evaluation of the enantiomer of synthesized molecules are important from a biocompatibility point of view since all plants or animals are made of only the left-handed molecules and the right-handed molecules might be sometimes harmful.

A single-wall carbon nanotube (SWNT) whose geometrical structure is specified by two integers, (n,m), belongs to either achiral [armchair (n,n) and zigzag $(n,0)$] or chiral [(n,m) with $n \neq m$ and $m \neq 0$] SWNTs [1–3]. In the case of the achiral SWNTs, the mirror image of an armchair (or a zigzag) nanotube by mirror operation parallel to the nanotube axis is identical to the original SWNT, while the mirror image of a chiral nanotube (n,m) is not the original (n,m) SWNT but another chiral nanotube $(n+m,-m)$ with different handedness [4]. Thus the CD spectra can be observed in the chiral SWNTs once one of enantiomers is separated from the sample. Since the mechanical or electronic properties of a pair of the enantiomer SWNTs are identical to each other, it is not possible to define and observe the handedness of SWNTs by conventional optical absorption spectra. It is important to evaluate the purity of one enantiomer in the SWNT sample by the measurement of optical activity combined with theoretical analysis of, e.g., CD spectra [5–12] or Raman optical activity spectra [13].

Measurements of the CD spectra for single chirality SWNTs have been reported in which separation of an enantiomer for a pair of chiralities [(n,m), and $(n+m,-m)$] is achieved by the agarose gel column chromatography method [5,7,10], the two-phase methods with DNA [6], use of the chiral surfactant diporphyrin [7–9], and the density gradient ultracentrifugation method with sodium cholate [10]. Liu *et al.* [5] and recently Wei *et al.* [11] adopted the allyl dextran-based gel for separation because the plant-based gel has a stronger interaction for the left-handed nanotubes (L-SWNTs) than the right-handed nanotubes (R-SWNTs). Here they propose a definition of L- and R-SWNTs by a minus and plus sign of CD values at E_{22} van Hove singularity energy, respectively. The reason why they select not E_{11} but E_{22} is that we usually measure E_{22} for the semiconductor SWNTs (s-SWNTs) in the visible-light range. In the case of the metallic SWNTs (m-SWNTs), we usually observe E_{11} which are split into E_{11}^{+} and E_{11}^{-} by the trigonal warping effect, except for the armchair SWNTs [14]. We will show that the CD values at E_{11}^{+} and E_{11}^{-} have opposite signs. Thus we will define L and R m-SWNTs as having positive and negative CD at E_{11}^{-} energy, respectively. Experimental results show that (1) opposite CD values are observed for a given wavelength for a pair of L-SWNT and R-SWNT, (2) the sign of the CD values for a L-SWNT (or a R-SWNT) oscillates at the van Hove singularity energies E_{ii} of the joint density of states [14], and (3) the signs of the CD at E_{ii} are opposite to each other for the type-I and type-II semiconductor chiral SWNTs. Here the metallic (m) SWNTs, the type-I and type-II semiconductor (s) SWNTs are defined by (n,m) SWNTs with $\mod(2n+m,3) = 0$, 1, and 2, respectively [14,15].

Sánchez-Castillo *et al.* reported the CD spectra for several chiralities such as (6,4), (6,5), and (8,4) by first-principles calculations [16,17]. Although they showed the alternating behavior of the calculated CD spectra as a function of the wavelength of light, they could not get a good agreement with experiment, simply because the purification of the enantiomer in the experiment that they used for the comparison was not good. Further, it would require long computational time by first-principles calculations if they calculated the CD spectra for chiral SWNTs with a large unit cell, which makes the investigation of chirality dependence of the CD spectra difficult, especially for a large unit cell of a chiral SWNT.

In this paper, we have calculated CD spectra of SWNTs by the tight binding method as a function of the wavelength. The tight binding method is convenient for discussing optical properties of graphene and nanotubes [18,19] since only the π orbitals of carbon atoms are relevant to the optical absorption in the visible-light range. The tight binding method will be able to

extend to CD spectra calculation with use of the exciton wave function, [20,21], although we do not adopt the exciton wave function in the present calculation for simplicity. In molecular quantum electrodynamics, CD of a molecule is expressed by the product of electric dipole moment and magnetic dipole moment [22] by considering not only electric dipole but also magnetic dipole interaction in the Hamiltonian, which is the lowest order of CD intensity of a molecule within the dipole approximation. If the size of a molecule is sufficiently small compared with the wavelength of incident light, phases of the electric field of the light for all atoms in the molecule can be taken to be the same for calculating the optical absorption, which is the dipole approximation. However, in the case of SWNTs, since the length (100–1000 nm) and/or diameter (2–3 nm) are not always negligibly small compared with the wavelength (500 nm), we discuss the difference of optical absorption using the CD angle θ in the order of 1 mdeg $= 10^{-5}$ rad, defined by

$$\tan\theta = \frac{I(\mathrm{RCP})^{1/2} - I(\mathrm{LCP})^{1/2}}{I(\mathrm{RCP})^{1/2} + I(\mathrm{LCP})^{1/2}}, \tag{1}$$

where $I(\mathrm{RCP})$ [$I(\mathrm{LCP})$] is the transmitted optical intensity for RCP (LCP) [5,10]. If we only consider the electric dipole moment, the CD value becomes zero within the dipole approximation. When we consider a correction term from the dipole approximation of an electric dipole, the term contributes to the CD spectra without considering the magnetic dipole term. It is noted that the dipole approximation works well when we discuss not the CD but the absolute value of optical absorption intensity.

In this paper, we will show that the phase of the light at each position of an atom in a SWNT, which is beyond the dipole approximation, gives the CD intensity of SWNTs. Thus we propose a theory of the CD spectra for SWNTs in this paper. The calculated results of the CD spectra as a function of the wavelength of light reproduce many aspects of experimental results.

Organization of the present paper is as follows. In Sec. II we present analytical formula for the CD of SWNTs within the tight binding method. In Sec. III numerical calculations of the CD spectra for type-I and -II s-SWNTs and m-SWNTs are given with a summary of the paper.

II. CIRCULAR DICHROISM OF A SWNT

Here we will show an analytical formula of the difference of optical absorption probability of a SWNT between the RCP and LCP within the tight binding method. When we consider the optical absorption intensity, we usually adopt the dipole approximation in which we assume the vector potential $\boldsymbol{A}$ as a constant in the calculation of electron-photon matrix elements $\langle\Psi_c|\boldsymbol{A}\cdot\nabla|\Psi_v\rangle \sim \boldsymbol{A}\cdot\langle\Psi_c|\nabla|\Psi_v\rangle$, in which Ψ_v and Ψ_c are, respectively, the wave functions of the valence and conduction bands (or π and π^* band) as the initial and final states, respectively. Here since we intentionally consider the phase factor of $\boldsymbol{A}$ at each site of carbon atoms in a SWNT, we will calculate not $\boldsymbol{A}\cdot\langle\Psi_c|\nabla|\Psi_v\rangle$ but $\langle\Psi_c|\boldsymbol{A}\cdot\nabla|\Psi_v\rangle$ to obtain the nonzero CD values.

The electronic structure of SWNTs is characterized by the chiral vector $\boldsymbol{C}_h = n\boldsymbol{a}_1 + m\boldsymbol{a}_2 \equiv (n,m)$, where $\boldsymbol{a}_1$ and $\boldsymbol{a}_2$ are unit vectors of the two-dimensional (2D) graphene [2,3]. The wave functions, Ψ_v and Ψ_c, are expressed by a linear combination of the Bloch functions for either the A or B carbon atom in the hexagonal unit cell of (hereafter hexagon) two-dimensional (2D) graphene [1] as follows:

$$\Psi_b(\boldsymbol{r},\boldsymbol{k}_b) = C_A^b(\boldsymbol{k}_b)\Phi_A(\boldsymbol{r},\boldsymbol{k}_b) + C_B^b(\boldsymbol{k}_b)\Phi_B(\boldsymbol{r},\boldsymbol{k}_b), \tag{2}$$

where the label $b = v$ or c denotes the valence or conduction band, respectively, and $C_A^b(\boldsymbol{k}_b)$ [$C_B^b(\boldsymbol{k}_b)$] is a coefficient of the Bloch function $\Phi_A(\boldsymbol{r},\boldsymbol{k}_b)$ [$\Phi_B(\boldsymbol{r},\boldsymbol{k}_b)$] as a function of wave vector $\boldsymbol{k}_b$. Since we consider the phase of light, we expect $\boldsymbol{k}_c \neq \boldsymbol{k}_v$ and $\boldsymbol{k}_c$ is given as a function of $\boldsymbol{k}_v$ in this paper. The Φ_ℓ ($\ell = A$ or B) is expressed by tight binding wave function of the $2p_z$ orbitals $\varphi(\boldsymbol{r})$ as follows:

$$\Phi_\ell(\boldsymbol{r},\boldsymbol{k}_b) = \frac{1}{\sqrt{U}}\sum_{m=1}^{U}\frac{1}{\sqrt{N}}\sum_{j=1}^{N}\exp\left(i\boldsymbol{k}_b\cdot\boldsymbol{R}_\ell^{j,m}\right) \times\varphi\left(\boldsymbol{r}-\boldsymbol{R}_\ell^{j,m}\right), \tag{3}$$

where U is the number of one-dimensional (1D) unit cells of the SWNT and $N = \sqrt{n^2+m^2+nm}$ is the number of hexagons in the 1D unit cell [1]. The vector $\boldsymbol{R}_\ell^{j,m} = \boldsymbol{R}_\ell^j + m\boldsymbol{T}$ is the position of the ℓth atom in the SWNT in which $\boldsymbol{T}$ is the translational vector of the SWNT and $\boldsymbol{R}_\ell^j$ denotes the position of the ℓth atom in the jth hexagon in the 1D unit cell [1]. The coefficients $C_\ell^b(\boldsymbol{k}_b)$ are calculated by solving the 2×2 Hamiltonian of graphene at $\boldsymbol{k} = \boldsymbol{k}_b$ in the 2D Brillouin zone in which the wave vector $\boldsymbol{k}$ is given by

$$\boldsymbol{k} = \mu\boldsymbol{K}_1 + k\frac{\boldsymbol{K}_2}{|\boldsymbol{K}_2|} \quad \left(\mu = 1,\ldots,N;\ -\frac{\pi}{T} < k < \frac{\pi}{T}\right), \tag{4}$$

where $\boldsymbol{K}_1$ and $\boldsymbol{K}_2$ denote, respectively, the reciprocal lattice vectors in the directions of circumferential and nanotube axes [1], and μ denotes the μth segments of N 1D Brillouin zones of the SWNT (hereafter we call them cutting lines [15,23]) in the 2D Brillouin zone of graphene as shown in Fig. 3, and T is the length of $\boldsymbol{T}$.

By the definition of CD, we calculate the difference of optical absorption intensity of the (n,m) SWNT between the RCP and LCP as

$$\Delta W(E_L) \equiv W_{-1}(E_L) - W_{+1}(E_L), \tag{5}$$

where $W_{-1}(E_L)$ and $W_{+1}(E_L)$ denote optical absorption probabilities as a function of the energy of light E_L, per unit time for RCP and LCP, respectively, and per unit length of the SWNT, each of which is given by the Fermi golden rule,

$$W_\sigma(E_L) \propto |\langle\Psi_c|\boldsymbol{A}_\sigma\cdot\nabla|\Psi_v\rangle|^2, \tag{6}$$

where σ is defined by an integer that specifies either RCP or LCP as follows:

$$\sigma = \begin{cases} -1 & (\mathrm{RCP}), \\ +1 & (\mathrm{LCP}). \end{cases} \tag{7}$$

Hereafter we set the axis of a SWNT in the direction of the z axis. When we consider $\boldsymbol{A}_\sigma$ as incident light, there are only two inequivalent propagating directions of the light ($\boldsymbol{q}$) as shown in Fig. 1; that is, (a) parallel to the nanotube axis ($\boldsymbol{q} \parallel \boldsymbol{T}$) and (b) perpendicular to the nanotube axis ($\boldsymbol{q} \perp \boldsymbol{T}$).

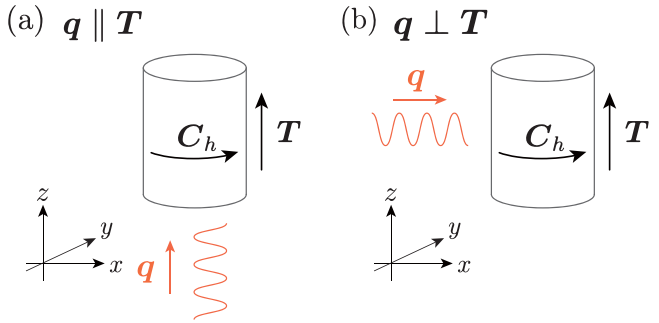

FIG. 1. Two geometries of propagating circular polarized light in the directions (a) parallel to the nanotube axis (z axis) and (b) perpendicular to the nanotube axis (x axis). The corresponding Jones vectors are given in Eq. (8).

The corresponding Jones vectors (the unit vector of $\boldsymbol{A}_\sigma$) are, respectively, given by

$$\mathbf{P}_\sigma^{\mathrm{3D}\parallel} = {}^t(i\sigma,1,0)/\sqrt{2} \quad \text{and} \quad \mathbf{P}_\sigma^{\mathrm{3D}\perp} = {}^t(0,i\sigma,1)/\sqrt{2}. \tag{8}$$

For the general propagating direction of circular polarized light, the Jones vector is given by the linear combination of $\mathbf{P}_\sigma^{\mathrm{3D}\parallel}$, $\mathbf{P}_\sigma^{\mathrm{3D}\perp}$, and ${}^t(1,0,i\sigma)/\sqrt{2}$.

In the calculation of Eq. (6), we consider an unrolled SWNT in which we redefine the vector potential $\boldsymbol{A}_\sigma$ at each atom [see Figs. 2(a) and 4(a)] on an unrolled plane as shown in Figs. 2(b), 2(c), and Figs. 4(b), 4(c). Figures 2 and 4 correspond to the cases of parallel and perpendicular propagation, respectively. If we plot $\boldsymbol{A}_\sigma$ on the unrolled plane, the vector potential is rotating by changing the position of the carbon atom. In this case, the perpendicular component of $\boldsymbol{A}_\sigma$ to the unrolled plane does not contribute to the matrix element [see Eqs. (A8) and (A10) in the Appendix]. Thus we consider only the in-plane component of $\boldsymbol{A}_\sigma$ which is expressed by $\boldsymbol{C}_h$ and $\boldsymbol{T}$. For convenience, we hereafter define unit vectors on *the unrolled plane* in the directions of $\boldsymbol{C}_h$ and $\boldsymbol{T}$ as

$$\boldsymbol{e}_C = \frac{\boldsymbol{C}_h}{L} \quad \text{and} \quad \boldsymbol{e}_T = \frac{\boldsymbol{T}}{T}, \tag{9}$$

where $L = |\boldsymbol{C}_h| = \pi d_t$ (d_t is the diameter of the SWNT [1]).

A. Propagation of light parallel to the SWNT axis

First we consider the optical absorption for the circular polarized light which propagates in the direction parallel to the nanotube axis ($\boldsymbol{q} \parallel \boldsymbol{T}$) as shown in Fig. 1(a). In the following calculation, we assume that the light does not become extinct in the direction of the nanotube axis (z) for simplicity. However, for any polarization directions of the light in the direction of x or y, the polarization vector can be tangential to a cylindrical surface of the SWNT from which we expect some extinction of the light in the z direction, which will not be discussed in this paper. In the case of $\boldsymbol{q} \parallel \boldsymbol{T}$, the in-plane component of polarization vector $\boldsymbol{P}_\sigma^\parallel$ at $\boldsymbol{R}_\ell^{j,m}$ defined on the unrolled SWNT is given by

$$\begin{aligned}\boldsymbol{P}_\sigma^\parallel\left(\boldsymbol{R}_\ell^{j,m}\right) &= \left(-i\sigma\sin\theta_j^\ell + \cos\theta_j^\ell\right)\boldsymbol{e}_C \\ &= \exp\left(-i\sigma\theta_j^\ell\right)\boldsymbol{e}_C,\end{aligned} \tag{10}$$

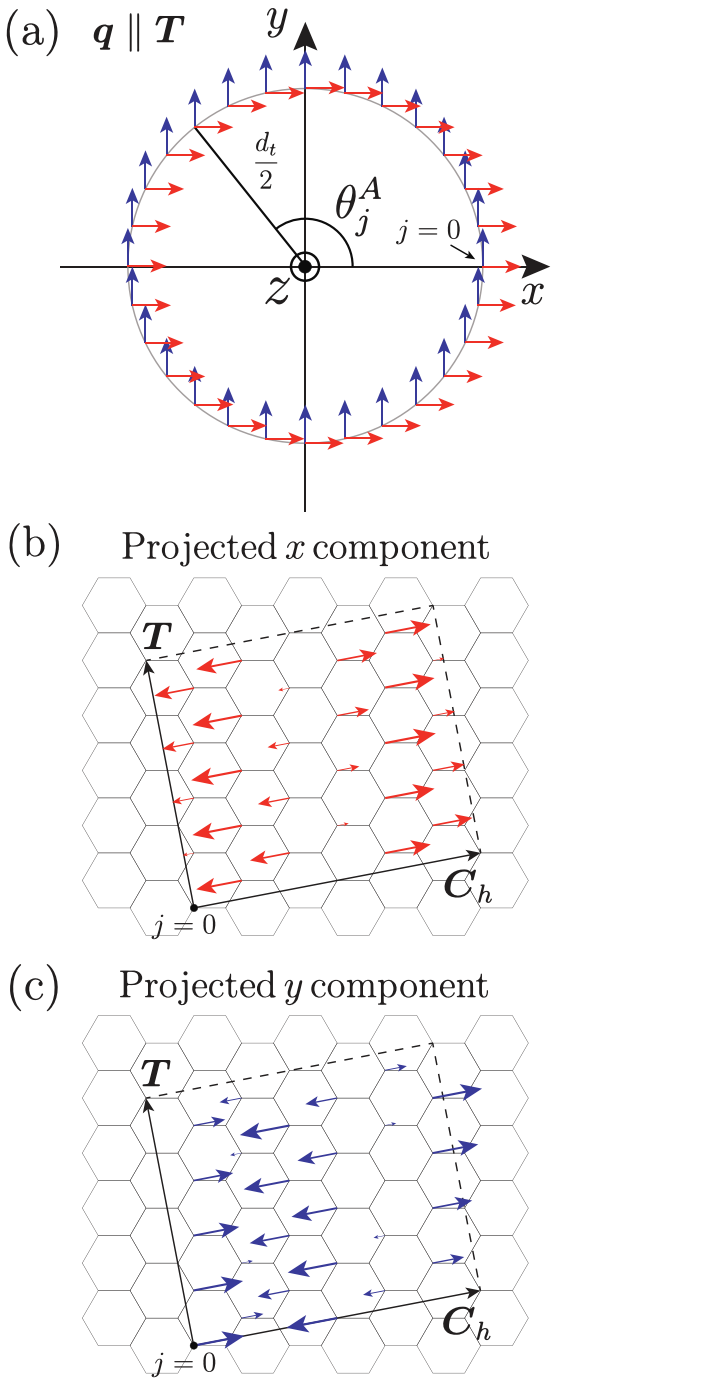

FIG. 2. Vector potential that propagates in the direction of z ($\boldsymbol{q} \parallel \boldsymbol{T}$) for a (4,2) SWNT ($N = 28$). (a) The Jones vector of light that propagates in the direction of z at each carbon site in the unit cell. We set the origin of coordinates at the 0th A atom in the 0th unit cell, $\boldsymbol{R}_A^{0,0}$, on the x axis, $\boldsymbol{R}_A^{0,0} = (d_t/2,0,0)$. The red and blue arrows correspond to x and y components, repsectively, of the Jones vector for the case of $\boldsymbol{q} \parallel \boldsymbol{T}$. (b) The x component and (c) the y component of vector potential projected on the unrolled plane. In the case of $\boldsymbol{q} \parallel \boldsymbol{T}$, only the $\boldsymbol{e}_C$ component of vector potential contributes to optical absorption [Eqs. (10) and (11)].

where the x and y components of $\boldsymbol{P}_\sigma^\parallel(\boldsymbol{R}_\ell^{j,m})$ for (4, 2) SWNT are shown in Figs. 2(b) and 2(c), respectively. The θ_j^ℓ is the angle of the ℓth atom of the jth hexagon measured from the

x axis as shown in Fig. 2(a). Using Eq. (10), we consider the vector potential with the phase factor of light for $\boldsymbol{q} \parallel \boldsymbol{T}$, $\boldsymbol{A}^{\parallel}_{\sigma,q}(\boldsymbol{R}^{j,m}_{\ell})$, where $q = |\boldsymbol{q}| = 2\pi/\lambda$ is the wave number of the light (λ is the wavelength) at $\boldsymbol{R}^{j,m}_{\ell}$ as follows:

$$\boldsymbol{A}^{\parallel}_{\sigma,q}\left(\boldsymbol{R}^{j,m}_{\ell}\right) = A\boldsymbol{P}^{\parallel}_{\sigma}\left(\boldsymbol{R}^{j,m}_{\ell}\right)\exp\left(iq\boldsymbol{e}_T\cdot\boldsymbol{R}^{j,m}_{\ell}\right), \tag{11}$$

where A is the amplitude of the vector potential. Here the origin of the phase of light is set to be zero at $z = 0$ and the time $t = 0$. Using Eqs. (2), (3), (10), and (11), we obtain the matrix element of optical absorption (see the Appendix, section 1, for the derivation) for the light propagating in the direction parallel to the SWNT axis as follows [18]:

$$\begin{aligned} M^{\parallel}_{\sigma}(\boldsymbol{k}_c,\boldsymbol{k}_v) &\equiv \langle\Psi_c(\boldsymbol{k}_c)|\boldsymbol{A}^{\parallel}_{\sigma,q}\left(\boldsymbol{R}^{j,m}_{\ell}\right)\cdot\nabla|\Psi_v(\boldsymbol{k}_v)\rangle \\ &= A\boldsymbol{e}_C\cdot\boldsymbol{C}(\boldsymbol{k}_c,\boldsymbol{k}_v)\delta\left(\boldsymbol{k}_c-\boldsymbol{k}^{\sigma}_c\right), \end{aligned} \tag{12}$$

where $\boldsymbol{k}^{\sigma}_c$ and $\boldsymbol{C}(\boldsymbol{k}_c,\boldsymbol{k}_v)$ are, respectively, defined by

$$\boldsymbol{k}^{\sigma}_c = \boldsymbol{k}_v - \sigma\boldsymbol{K}_1 + \tau\boldsymbol{K}_2, \tag{13}$$

$$\boldsymbol{C}(\boldsymbol{k}_c,\boldsymbol{k}_v) = \frac{2\sqrt{3}m_{\rm opt}}{a}\mathrm{Re}\left[C^{c*}_A(\boldsymbol{k}_c)C^{v}_B(\boldsymbol{k}_v)\boldsymbol{Z}_A\right]. \tag{14}$$

Here $\tau = T/\lambda$ is the ratio of T to the wavelength of light λ and $\boldsymbol{Z}_A$ is defined in Eq. (A9). It is important to note that $\boldsymbol{k}^{\sigma}_c$ depends on τ and σ. Hereafter we denote $\boldsymbol{k}^{+}_c$ and $\boldsymbol{k}^{-}_c$ for $\sigma = +1$ and $\sigma = -1$, respectively for avoiding the confusion of the inversion. Since the direction of the electric field (x or y) is perpendicular to the nanotube axis z, an angular momentum of either $\boldsymbol{K}_1$ or $-\boldsymbol{K}_1$ is added to $\boldsymbol{k}^{\sigma}_c$ in the delta function of Eq. (12) as the momentum conservation for $\sigma = -1$ or $+1$, respectively [see Fig. 3(a)]. Further, additional momentum $\tau\boldsymbol{K}_2$ which depends on λ appears in the expression of $\boldsymbol{k}^{\sigma}_c$ when we consider the phase of the vector potential. Since the $\boldsymbol{k}^{\sigma}_c$'s for RCP and LCP are different from each other for a given $\boldsymbol{k}_v$, the optical transition probabilities for RCP and LCP for a given $\boldsymbol{k}_v$ are different from each other, too.

Using Eq. (12), the difference of optical absorption at $\boldsymbol{k}_v$ for given E_L is obtained from the Fermi golden rule as follows:

$$\begin{aligned} \Delta W^{\parallel}_{\rm RL}(E_L,\boldsymbol{k}_v) \equiv{}& \left|M^{\parallel}_{-1}(\boldsymbol{k}^{-}_c,\boldsymbol{k}_v)\right|^2\delta(E_L-E^{-}_{cv}) \\ &-\left|M^{\parallel}_{+1}\left(\boldsymbol{k}^{+}_c,\boldsymbol{k}_v\right)\right|^2\delta(E_L-E^{+}_{cv}), \end{aligned} \tag{15}$$

where $E^{\sigma}_{cv} = E_c(\boldsymbol{k}^{\sigma}_c) - E_v(\boldsymbol{k}_v)$ is the energy gap between the initial and final states where $E_c(\boldsymbol{k}^{\sigma}_c)$ and $E_v(\boldsymbol{k}_v)$ are energies of conduction and valence energy bands at $\boldsymbol{k}^{\sigma}_c$ and $\boldsymbol{k}_v$, respectively. We note that $M^{\parallel}_{\sigma}(\boldsymbol{k}^{\sigma}_c,\boldsymbol{k}_v)$ with different $\boldsymbol{k}_v$ contributes to the CD of a given E_L for $\sigma = \pm 1$. The CD intensity as a function of E_L is calculated by integrating Eq. (15) on $\boldsymbol{k}_v$ in the 2D Brillouin zone for all cutting lines defined by Eq. (4) as follows:

$$\Delta W^{\parallel}(E_L) = \sum_{\mu=1}^{N}\int_{-\pi/T}^{\pi/T}\Delta W^{\parallel}_{\rm RL}(E_L,\boldsymbol{k}_v)dk_v. \tag{16}$$

In the numerical calculation, we take a summation on all cutting lines and k points on each cutting line with the

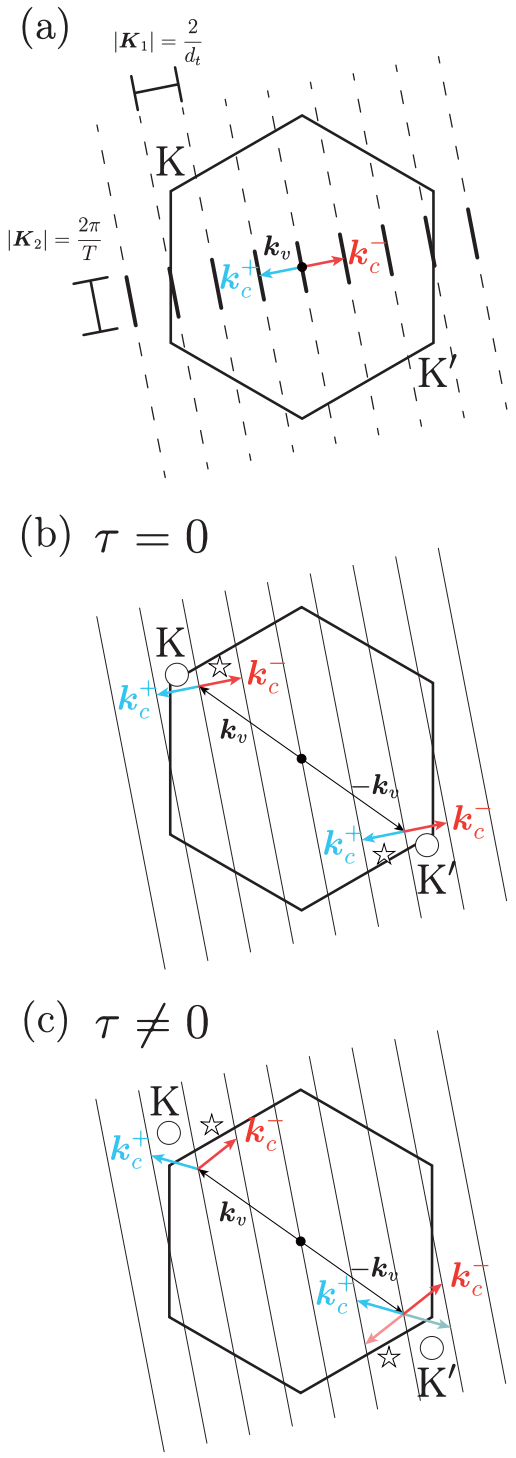

FIG. 3. (a) Cutting lines of SWNT and the selection rule of optical absorption for RCP (red arrow) and LCP (blue arrow) for the case of the incident light parallel to the nanotube axis. (b),(c) The selection rule for optical absorption (b) without and (c) with considering the optical phase factor $\tau\boldsymbol{K}_2$. In the case of (b) $\tau = 0$, the optical transition around the K point that are shown by either the red arrow [star (RCP)] or the blue arrow [circle (LCP)] are identical, respectively, to the blue arrow [star (LCP)] or red arrow [circle (RCP)] around the K' point, which would give zero CD values. (c) If we consider the effect of the phase factor of light ($\tau \neq 0$), the arrows tilt from the perpendicular direction in the same direction ($\tau\boldsymbol{K}_2$), and thus the cancellation between either circle or star does not occur.

same density in the k space for all (n,m) SWNTs, which corresponds the fact that CD intensity is normalized by the length of the SWNTs. We take 100 k points on each cutting line for calculating the CD of a (6,4) SWNT. It is important to note that the additional momentum $\tau \boldsymbol{K}_2$ in the direction of the nanotube axis appears in Eq. (13) as an effect of the phase of the light. In fact, in the limit of $\lambda \to \infty$, we get $\tau = 0$.

When $\tau = 0$, the momentum difference of $\boldsymbol{k}_c - \boldsymbol{k}_v = -\sigma \boldsymbol{K}_1$ is perpendicular to the cutting lines ($\boldsymbol{K}_2$) as shown in Fig. 3(a). In this case, the optical transition probability near the K point for RCP (LCP) that is shown as a star (circle) in Fig. 3(b) is identical to that near the K' point for LCP (RCP). Thus even though the two transitions by RCP and LCP for a given $\boldsymbol{k}_v$ are different from each other, the difference of optical transition probability becomes zero by canceling the transitions near the K and K' points when we integrate the probability over the 2D Brillouin zone. However, when we consider the effect of τ, the momentum difference is no longer perpendicular to the cutting line as shown in Fig. 3(c); the momentum vectors for LCP and RCP tilt in the same direction for a given $\boldsymbol{k}_v$ and for K and K' points. In such a situation, the cancellation between K and K' does not occur. Thus this effect of τ is essential for obtaining the finite values of CD in SWNTs.

B. Propagation of light perpendicular to SWNT axis

When propagating direction of light is perpendicular to the nanotube axis ($\boldsymbol{q} \perp \boldsymbol{T}$) as shown in Fig. 1(b), the projected y and z components of polarization vector $\boldsymbol{P}_\sigma^\perp$ at $\boldsymbol{R}_\ell^{j,m}$ are given by [see Figs. 4(b) and 4(c)]

$$\boldsymbol{P}_\sigma^\perp\left(\boldsymbol{R}_\ell^{j,m}\right) = i\sigma \cos\theta_j^\ell \boldsymbol{e}_C + \boldsymbol{e}_T. \tag{17}$$

The phase of the vector potential at the ℓth atom in the jth hexagon in the 1D unit cell ($\boldsymbol{R}_\ell^{j,m}$) depends on θ_j^ℓ, while the phase does not depend on T. In this case, the vector potential at $\boldsymbol{R}_\ell^{j,m}$, $\boldsymbol{A}_{\sigma,q}^\perp(\boldsymbol{R}_\ell^{j,m})$, can be expressed by sum of the components in the direction of $\boldsymbol{e}_C$ and $\boldsymbol{e}_T$ [see Figs. 4(b) and 4(c)] as follows:

$$\boldsymbol{A}_{\sigma,q}^\perp\left(\boldsymbol{R}_\ell^{j,m}\right) = i\sigma A_q^C\left(\boldsymbol{R}_\ell^{j,m}\right)\boldsymbol{e}_C + A_q^T\left(\boldsymbol{R}_\ell^{j,m}\right)\boldsymbol{e}_T, \tag{18}$$

where $A_q^C(\boldsymbol{R}_\ell^{j,m})$ and $A_q^T(\boldsymbol{R}_\ell^{j,m})$ are the coefficients of the vector potential for the directions of $\boldsymbol{C}_h$ and T, respectively. When we put the origin of the phase of the incident light at $x = 0$ as shown in Fig. 4(a), $A_q^C(\boldsymbol{R}_\ell^{j,m})$ and $A_q^T(\boldsymbol{R}_\ell^{j,m})$ are given by

$$A_q^C\left(\boldsymbol{R}_\ell^{j,m}\right) = A\cos\theta_j^\ell\left(1 + i\beta\cos\theta_j^\ell\right), \tag{19}$$

$$A_q^T\left(\boldsymbol{R}_\ell^{j,m}\right) = A\left(1 + i\beta\cos\theta_j^\ell\right), \tag{20}$$

where $\beta \equiv \pi d_t/\lambda = q d_t/2$ is the phase of light. When we consider the phase of the vector potential of the jth B atom, we multiply a constant factor, $\exp(i\boldsymbol{K}_1 \cdot \boldsymbol{r}_A^1)$, to that of jth A atom, where $\boldsymbol{r}_A^1 = (\boldsymbol{a}_1 + \boldsymbol{a}_2)/3$ is the nearest neighbor vector from the jth A atom to the jth B atom.

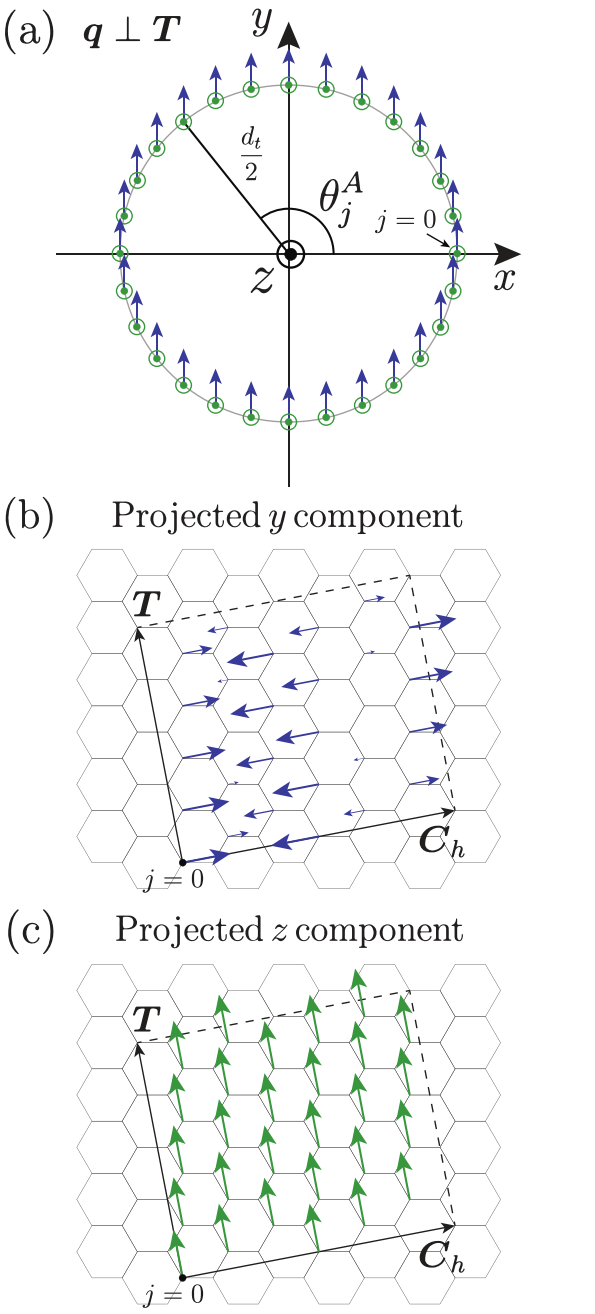

FIG. 4. (a) The Jones vector of light that propagates in the direction of x for (4,2) SWNTs. We put the 0th A atom at $\boldsymbol{R}_A^{0,0} = (d_t/2,0,0)$. The blue and green arrows correspond to y and z components, respectively, of the Jones vector for the case of $\boldsymbol{q} \perp \boldsymbol{T}$. (b) The y and (c) z components of the vector potential defined on unrolled SWNT plane. In the case of $\boldsymbol{q} \perp \boldsymbol{T}$, the Jones vector has both of $\boldsymbol{e}_C$ and $\boldsymbol{e}_T$ components. The $\boldsymbol{e}_C$ component exists in the y component where the absolute value and the sign depend on $\boldsymbol{R}_\ell^{j,m}$, while the $\boldsymbol{e}_T$ component exists in the z component that does not depend on $\boldsymbol{R}_\ell^{j,m}$.

From Eqs. (19) and (20), the electron-photon matrix element for the case of $\boldsymbol{q} \perp \boldsymbol{T}$ is given as follows (see the

Appendix, section 2, for the derivation):

$$M_{\sigma}^{\perp}(\boldsymbol{k}_c,\boldsymbol{k}_v) \equiv \langle \Psi_c(\boldsymbol{k}_c)|\boldsymbol{A}_{\sigma,q}^{\perp}\left(\boldsymbol{R}_{\ell}^{j,m}\right)\cdot\nabla|\Psi_v(\boldsymbol{k}_v)\rangle$$
$$= A\boldsymbol{C}(\boldsymbol{k}_v,\boldsymbol{k}_c)\cdot\left[\left(-\sigma\frac{\beta}{2}\boldsymbol{e}_C+\boldsymbol{e}_T\right)\delta(\boldsymbol{K})\right.$$
$$+\frac{i}{2}(\sigma\boldsymbol{e}_C+\beta\boldsymbol{e}_T)\{\delta(\boldsymbol{K}-\boldsymbol{K}_1)+\delta(\boldsymbol{K}+\boldsymbol{K}_1)\}$$
$$\left.-\sigma\frac{\beta}{4}\boldsymbol{e}_C\{\delta(\boldsymbol{K}-2\boldsymbol{K}_1)+\delta(\boldsymbol{K}+2\boldsymbol{K}_1)\}\right], \tag{21}$$

where $\boldsymbol{K}\equiv\boldsymbol{k}_c-\boldsymbol{k}_v$. It is noted that $\boldsymbol{k}_c$ does not depend on σ in the case of $\boldsymbol{q}\perp\boldsymbol{T}$. In Eq. (21), there are three selection rules for $\boldsymbol{k}_c$: (a) $\boldsymbol{k}_c=\boldsymbol{k}_v$ (the same cutting line), (b) $\boldsymbol{k}_c=\boldsymbol{k}_v\pm\boldsymbol{K}_1$ (the nearest neighbor cutting lines), (c) $\boldsymbol{k}_c=\boldsymbol{k}_v\pm2\boldsymbol{K}_1$ (the second nearest neighbor cutting lines). The case of (c) appears since there is a term of $\cos^2\theta_j^{\ell}=(1+\cos2\theta_j^{\ell})/2$ in Eq. (19), which gives twice the angular momentum as the term of $\cos2\theta_j^{\ell}$. The phase factor β appears in both directions of $\boldsymbol{e}_C$ and $\boldsymbol{e}_T$. The difference of optical absorption $\Delta W_{\mathrm{RL}}^{\perp}$ is defined by

$$\Delta W_{\mathrm{RL}}^{\perp}(E_L,\boldsymbol{k}_v)$$
$$\equiv(|M_{-1}^{\perp}(\boldsymbol{k}_c,\boldsymbol{k}_v)|^2-|M_{+1}^{\perp}(\boldsymbol{k}_c,\boldsymbol{k}_v)|^2)\delta(E_L-E_{cv})$$
$$= A^2\beta[\boldsymbol{e}_C\cdot\boldsymbol{C}(\boldsymbol{k}_c,\boldsymbol{k}_v)][\boldsymbol{e}_T\cdot\boldsymbol{C}(\boldsymbol{k}_c,\boldsymbol{k}_v)]$$
$$\times[2\delta(\boldsymbol{K})-\delta(\boldsymbol{K}+\boldsymbol{K}_1)-\delta(\boldsymbol{K}-\boldsymbol{K}_1)]\delta(E_L-E_{cv}), \tag{22}$$

where $E_{cv}\equiv E_c(\boldsymbol{k}_c)-E_v(\boldsymbol{k}_v)$ is the energy gap between the initial and final states. The derivation of Eq. (22) is given in the Appendix, section 2, too. It is clear from Eq. (22) that we get $\Delta W_{\mathrm{RL}}^{\perp}=0$ when $\beta=0$. It is noted that the crossing terms such as $\delta(\boldsymbol{K})\delta(\boldsymbol{K}+\boldsymbol{K}_1)$ disappear because of the product of different delta functions on $\boldsymbol{K}$. Further, the term of $\delta(\boldsymbol{K}\pm2\boldsymbol{K}_2)$ disappears in Eq. (22) because there is no linear σ term after taking the square.

The CD intensity as a function of E_L is calculated by integrating Eq. (22) on $\boldsymbol{k}_v$ in the 2D Brillouin zone for all cutting lines as follows:

$$\Delta W^{\perp}(E_L)=\sum_{\mu=1}^{N}\int_{-\pi/T}^{\pi/T}\Delta W_{\mathrm{RL}}^{\perp}(E_L,\boldsymbol{k}_v)dk_v. \tag{23}$$

III. RESULTS AND DISCUSSION

In Fig. 5, we plot the CD angles of the perpendicular geometry defined by Eq. (1) as a function of the wavelength for (a) (6,4), (b) (6,5), (c) (7,6), and (d) (9,6) SWNTs. In Fig. 5, we also show the experimental data of CD taken from the published papers [11,12]. Since most of the experimental CD spectra are given as a function of wavelength λ, we use a conversion of $E_L=hc/\lambda$ where h and c are the Planck constant and the velocity of light, respectively. In order to compare the calculated results with the experimental results quantitatively, we formulate the relationship between ΔW and CD as follows. The intensities of the transmitted light for RCP and LCP in Eq. (1) are defined by the Beer-Lambert law as follows:

$$I(\mathrm{RCP})=I_0 10^{-A_R}, \tag{24}$$

$$I(\mathrm{LCP})=I_0 10^{-A_L}, \tag{25}$$

where I_0 and A_R (A_L) are the intensity of the incident light and the absorbance for RCP (LCP), respectively. Using Eqs. (1), (24), and (25), the CD angle is given as a function of

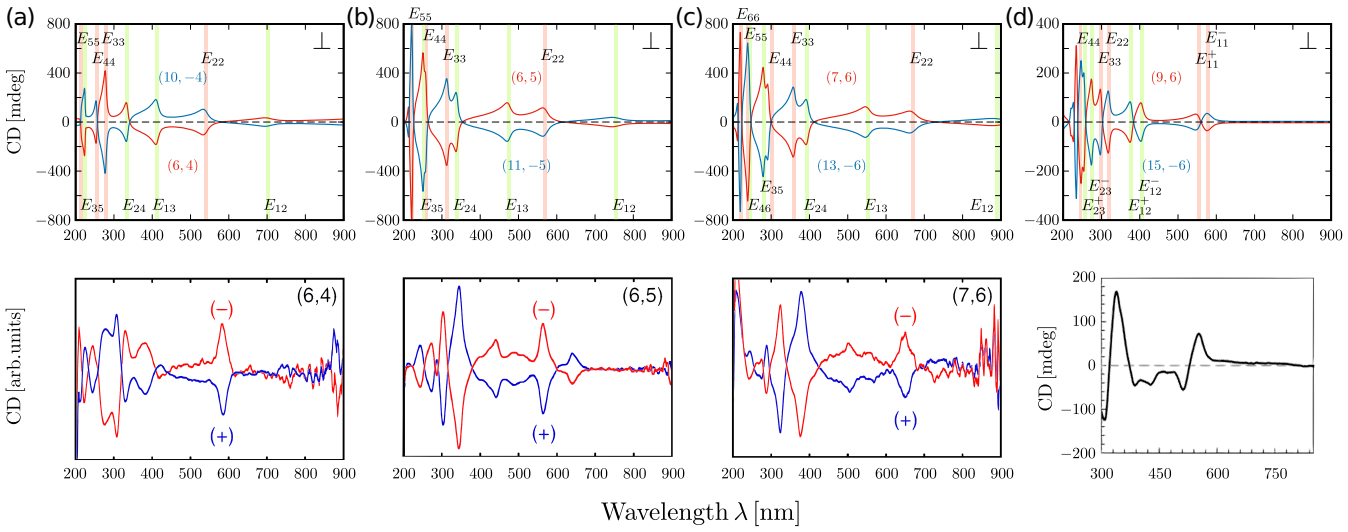

FIG. 5. In the top row, the calculated CD intensities of the perpendicular [$\mathrm{CD}^{\perp}(\lambda)$] case for (a) (6,4) (red lines) and (10,−4) (blue) type-I s-SWNTs, (b) (6,5) (red) and (11,−5) (blue) type-II s-SWNTs, (c) (7,6) (red) and (13,−6) (blue) type-II s-SWNTs, and (d) (9,6) (red) and (15,−6) (blue) m-SWNTs. Here we adopt $x=1$ μg/ml and $L=1$ cm. Van Hove singular transitions energies at E_{ij} are shown in the vertically shaded area. Experimental data taken from Refs. [11] for s-SWNTs and [12] for m-SWNTs are shown in the bottom. The colors in the experiments do not correspond to the calculated results. As for (9,6) m-SWNT, only one CD spectra is shown and the horizontal axis is from 300 to 850 nm.

the difference of the absorbance $\Delta A = A_R - A_L$ as follows:

$$\mathrm{CD} = \theta = \frac{180\,000}{4\pi \log_{10} e} \times \Delta A \ (\mathrm{mdeg}). \tag{26}$$

ΔA is expressed by the product of the difference of the absorption coefficient $\Delta\alpha$ and the light path length L, that is, $\Delta A = \Delta\alpha \times L$. The relationship between ΔA and the transition probabilities ΔW ($= \Delta W^{\parallel}$ or $\Delta W^{\perp}$) which are defined in Eqs. (16) or (23), respectively is given by

$$\Delta A = \frac{2\pi e^2\hbar^2}{\epsilon_0\epsilon_r {m_e}^2 \omega c}\frac{L}{V}\Delta W(E_L), \tag{27}$$

where m_e, ω, and V are the mass of electron, the angular frequency of the incident light, and the volume of the sample, respectively. Since the experimental CD values of SWNTs are measured in the solution, we use the dielectric constant of water $\varepsilon_r = 80$. For evaluating CD values, we need the mass concentration of the carbon atoms x which is given by

$$x = \frac{2NM_C}{VN_A}, \tag{28}$$

where $2N$, N_A, and $M_C = 12$ are the number of carbon atoms in the unit cell, Avogadro's constant, and the mass number of carbon, respectively. Then the experimantal absorption coefficient in the solution ΔA_{exp} is given by

$$\begin{aligned}\Delta A_{\mathrm{exp}} &= \frac{x_{\mathrm{exp}}\Delta A}{x} \\ &= x_{\mathrm{exp}}\frac{\pi e^2\hbar^2 N_A L}{\epsilon_0\epsilon_r {m_e}^2 \omega c N M_C}\Delta W(E_L),\end{aligned} \tag{29}$$

where x_{exp} is the mass concentration of the SWNTs in the solution adopted in the experimental condition. Since we did not know the experimental values of x_{exp} and the path of light L, we asked one of the coauthors of Ref. [11] for the values. Hence we obtained the values of the mass concentration $x_{\mathrm{exp}} \sim 1$ (μg/ml) and light path $L = 1$ (cm) that are needed for calculating CDs in Fig. 5. Furthermore, we need to consider the enhancement of the electron-photon matrix element by the exciton effect that is considered by Jiang et al. [20,21]. Since our calculation and Jiang's calculation are based on the same tight-binding method, we can simply adopt the enhancement factor of Jiang *et al.* Here we adopt the ratios of the exciton-photon to the electron-photon matrix element at the E_{22} peak as $M_{\text{ex-op}}/M_{\text{el-op}} = 10.5$ for m-SWNT, and $M_{\text{ex-op}}/M_{\text{el-op}} = 15.4$ for s-SWNTs [20].

By comparing the calculated spectra with experimental spectra in Fig. 5, we notice that peaks of the calculated CD at E_{12} or E_{13} etc. that are strong for $\Delta W^{\parallel}$ do not appear in the experiment. To explain this situation, we show $\Delta W^{\parallel} \propto \mathrm{CD}^{\parallel}$ and $\Delta W^{\perp} \propto \mathrm{CD}^{\perp}$ in the supplemental information. There are many possible reasons why we do not see $\mathrm{CD}^{\parallel}$ or $\Delta W^{\parallel}$ in the experiment, such as (1) the light propagating in the direction of the nanotube axis may become extinct along the CNT axis, (2) a depolarization effect for perpendicular polarization to the cylindrical surface suppresses the absorption [24,25], and (3) there are relatively weak exciton effects for E_{12} or E_{13} compared with E_{11} [26]. Regarding the extinction of light, there are carbon atoms that get the in-plane electric field in any direction of polarization. Thus we expect 2.3% optical absorption for the carbon atoms. The extinction of light can be measured by experiment if we align SWNTs, which should be a future goal. It is beyond the purpose of the present paper to investigate the exciton effect for CD values.

A pair of (n,m) and $(n+m,-m)$ for each figure in Fig. 5 are enantiomers to each other. The vertically shaded areas in each figure correspond to the energy regions of the van Hove singularity of the joint density of states, E_{ii} or E_{ij}, for the SWNTs. For the optical transition within the same cutting line, the energy regions of E_{11}, E_{22}, E_{33}, etc. are relevant to the CD spectra, while for the optical transition between nearest neighbor cutting lines the regions of E_{12}, E_{13}, E_{24}, and E_{35} are relevant (see Fig. 6).

The calculated result of Fig. 5(a) [or 5(b), 5(c)] shows that CD gives the opposite sign with the same absolute values between (6,4) and (10,−4) [or (6,5) and (11,−5), (7,6), and (13,−6)]. From the definition of Eq. (5), we get

$$\begin{aligned}&\Delta W(n,m,E_L) \\ &\quad\equiv W_{-1}(n,m,E_L) - W_{+1}(n,m,E_L) \\ &\quad= W_{+1}(n+m,-m,E_L) - W_{-1}(n+m,-m,E_L) \\ &\quad= -\Delta W(n+m,-m,E_L),\end{aligned} \tag{30}$$

where $\Delta W(n,m,E_L)$ denotes $\Delta W(E_L)$ for (n,m) SWNTs. From the second line to the third line in Eq. (30), we use the fact that the physical properties of the optical transition probability give the same values for (1) L-SWNT for LCP (or RCP) and (2) R-SWNT for RCP (or LCP) due to the mirror symmetry between (a) LCP and RCP or (b) L-SWNT and R-SWNT. It is clear from Eq. (30) that zigzag nanotubes, $(n,0)$ $(m = 0)$, or armchair nanotubes, (n,n) $(n = m)$, give no CD spectra ($\Delta W = 0$), since the enantiomer of $(n,0)$ or (n,n) for the achiral nanotubes is identical to the original $(n,0)$ or (n,n) SWNTs [$(2n,n) \equiv (n,n)$ by 60° rotation]. Thus from Eq. (30) we get $\Delta W(n,0,E_L) = -\Delta W(n,0,E_L)$ for $(n,0)$ which means $\Delta W(n,0,E_L) = 0$.

In Figs. 6(a), 6(b), and 6(c), we show the cutting lines near the K point, respectively, for type-I and -II s-SWNTs and m-SWNTs; we show the optical transition of E_{ij} in which the cutting lines are numbered from the closest to the K point. The E_{ii} transition corresponds to the transition within the ith cutting line measured from the K (K') point. According to the definition of type-I and -II s-SWNTs, the K point is located at (a) $(p+1/3)\boldsymbol{K}_1$, (b) $(p+2/3)\boldsymbol{K}_1$, (c) $p\boldsymbol{K}_1$ for type-I and -II SWNTs and for m-SWNTs, respectively, where p is an integer. In this case, we expect that CD values of E_{11} (E_{22}) for a type-I SWNT may have the same sign as those of E_{22} (E_{11}) for a type-II SWNT, since the corresponding $\boldsymbol{k}_c$ and $\boldsymbol{k}_v$ positions are on the same side relative to the K point in the Brillouin zone.

This is the reason why type-I and -II R-SWNTs (or L-SWNTs) such as (6,4), (6,5), and (7,6) have the opposite values for a given E_{ii}. In the case of m-SWNT, one cutting line goes over the K point and two nearest cutting lines 1+ and 1− in Fig. 6(c) contribute to the E_{11} transition energy. In this case, because of trigonal warping effect of equi-energy lines [14], E_{11} energies are split into E_{11}^{+} and E_{11}^{-} in which E_{11}^{+} corresponds to the 1+ cutting line inside of the Brillouin zone, while E_{11}^{-} corresponds to the 1− cutting line outside of

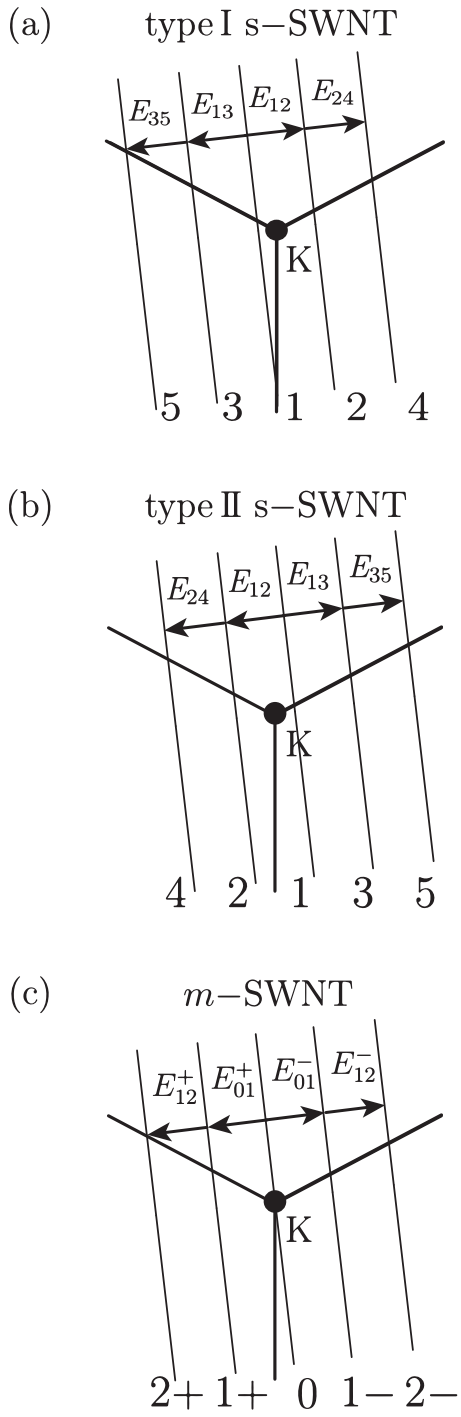

FIG. 6. Cutting lines for (a) type-I s-SWNTs, (b) type-II s-SWNT, and (c) m-SWNT. The cutting lines are numbered from the closest one to the K point. E_{ij} denote the two cutting lines that contribute to the E_{ij} van Hove singularity.

the Brillouin zone. Because of a similar reason for s-SWNTs, CD values for E_{11}^{+} and E_{11}^{-} are opposite values to each other. This is consistent with the fact that the CD value at E_{11}^{-} for a (9,6) m-SWNT and E_{22} for a (6,4) type-I s-SWNT have the same signs for $\boldsymbol{q} \perp \boldsymbol{T}$, since these cutting lines are located at the outside of the Brillouin zone. In the case of $\boldsymbol{q} \parallel \boldsymbol{T}$, $\Delta W^{\parallel}$ does not change the sign for E_{11}^{-} and E_{11}^{+} (see Supplemental Material [27]). The reason for this is understood by Eq. (12), in which $W_{\sigma}^{\parallel} = |M_{\sigma}^{\parallel}(\boldsymbol{k}_c^{\sigma}, \boldsymbol{k}_v)|^2$ is proportional to the square of $C(\boldsymbol{k}_c^{\sigma}, \boldsymbol{k}_v)$, which does not change the sign inside or outside of the Brillouin zone. In Table I, we list our definition of L-SWNT and R-SWNT by the sign of CD values at E_{22} energy for type-I and type-II s-SWNTs and at E_{11}^{-} energy for m-SWNTs. For a conventional (n,m) SWNT with $0 < m < n$, we define it as L-SWNT. It is noted that the definition of L and R can be exchanged if we change how we roll up the graphene sheet into a cylinder in either z or $-z$ sides, depending on the rolled up 1D unit cell as shown in Fig. 2. Here we adopt the $-z$ side for the definition.

TABLE I. Definition of L-SWNT (L) and R-SWNT (R) by sign of CD values at E_{22} energy for type-I and type-II s-SWNTs and at E_{11}^{-} energy for m-SWNT.

	E_{22} of s-SWNT		
	type-I	type-II	E_{11}^{-} of m-SWNT
CD > 0	R	L	R
CD < 0	L	R	L

We note that the peak positions of CD values are not exactly matched to E_{ij} (E_{ii}) values especially for larger λ (or lower E_L). In the case of CD$^{\perp}$, the effect of β in Eq. (22) changes the peak position of CD from E_{ii} (E_{ij}) values. For smaller λ (or larger E_L), the energy dispersion far from the K point gradually becomes flat and thus the deviation of CD peaks from E_{ii} (E_{ij}) energy becomes smaller. Since this deviation affects the shape of energy dispersion on the cutting lines, that depends on the distance from the K point or chiral angle, the effect should be large for larger d_t (smaller $|\boldsymbol{K}_1|$) for a given λ, which means small separation between two nearest neighbor cutting lines or for angles closer to the armchair chiral angle.

The calculated results of CD spectra are similar to the calculated results by first principles [16,17]. However, if we adopt the dipole approximation for the conventional theory of CD, we get zero CD values after taking integration over the Brillouin zone as discussed in Sec. III A. In Ref. [17], since the authors did geometrical optimization of the lattice which makes the symmetry lower, this might be a reason why they got nonzero results and values similar to the present results even though they did not consider the exciton effect.

Before finishing the discussion, we point out that CD values increase with decreasing λ, which is consistent with the experimental results [5–11,13]. This fact can be understood that both the τ and β terms in Eqs. (13), (19), and (20) are inversely proportional to λ. Thus the phase shift effect seems to be essential for understanding CD for chiral SWNTs. It should be mentioned that we did not consider the exciton effect as a function of the wavelength, but we adopt a constant enhancement factor. Thus further investigation is needed to take into account the exciton effect as a function of the wavelength.

In conclusion, we formulate CD values of chiral SWNTs, in which the phase difference effects expressed by τ or β are important to understand the λ or type dependence of CD spectra. In order to discuss the contribution for CD$^{\perp}$ and CD$^{\parallel}$, we should consider many other effects such as

extinction of light, depolarization effects [24,25], or exciton effects [20,21,26], which will be a future problem. Although the present paper does not investigate the detailed effects, the physics of CD in SWNTs are explained in analytic form.

ACKNOWLEDGMENTS

R.S. acknowledges Dr. X. Wei, Dr. H. Kataura, and Prof. M. Cheng for valuable discussions and for showing many unpublished experimental data. R.S. acknowledges JSPS KAKENHI (Grants No. JP25286005 and No. JP25107005) and the late Prof. M. S. Dresselhaus for discussions.

APPENDIX

In this appendix, we derive the analytical formula of the difference of the optical absorption probabilities between RCP and LCP for light propagating in the direction ($\boldsymbol{q}$) of parallel and perpendicular incident light to the SWNT axis ($\boldsymbol{T}$). The matrix elements of the electron-photon interaction are given by

$$M_\sigma(\boldsymbol{k}_c,\boldsymbol{k}_v) = \langle\Psi_c(\boldsymbol{k}_c)|\boldsymbol{A}_{\sigma,q}(\boldsymbol{r})\cdot\nabla|\Psi_v(\boldsymbol{k}_v)\rangle, \tag{A1}$$

and we evaluate Eq. (A1) for the cases of (1) $\boldsymbol{q}\parallel\boldsymbol{T}$ and (2) $\boldsymbol{q}\perp\boldsymbol{T}$.

1. Propagation of light parallel to nanotube axis

In the case of $\boldsymbol{q}\parallel\boldsymbol{T}$, the vector potential defined on unrolled graphene is given in Eq. (11) and Fig. 2,

$$\boldsymbol{A}^{\parallel}_{\sigma,q}\left(\boldsymbol{R}^{j,m}_{\ell}\right) = A\exp\left\{i\left(q\boldsymbol{e}_T\cdot\boldsymbol{R}^{j,m}_{\ell}-\sigma\theta^{\ell}_j\right)\right\}\boldsymbol{e}_C, \tag{A2}$$

where $q=2\pi/\lambda$ is the wave number of light and θ^{ℓ}_j is the angle for the position of the ℓth carbon atom in the jth hexagon as shown in Fig. 2(a). The lattice vector for the ℓth carbon atom in the jth hexagon of the mth unit cell in a SWNT is given by

$$\boldsymbol{R}^{j,m}_{\ell} = \boldsymbol{R}^{j}_{\ell}+m\boldsymbol{T}\quad(j=0,\ldots,N-1). \tag{A3}$$

By using Eqs. (2), (A1), and (A2), the matrix element of electron-photon interaction for $\boldsymbol{q}\parallel\boldsymbol{T}$ is given by

$$\begin{aligned}M^{\parallel}_{\sigma}(\boldsymbol{k}_c,\boldsymbol{k}_v) &= \langle\Psi_c(\boldsymbol{k}_c)|\boldsymbol{A}^{\parallel}_{\sigma,q}\left(\boldsymbol{R}^{j,m}_{\ell}\right)\cdot\nabla|\Psi_v(\boldsymbol{k}_v)\rangle\\ &= AC^{c*}_A(\boldsymbol{k}_c)C^{v}_B(\boldsymbol{k}_v)\boldsymbol{D}^{AB}\cdot\boldsymbol{e}_C\\ &\quad + AC^{c*}_B(\boldsymbol{k}_c)C^{v}_A(\boldsymbol{k}_v)\boldsymbol{D}^{BA}\cdot\boldsymbol{e}_C,\end{aligned} \tag{A4}$$

where we define the dipole vectors from B (A) to A (B) atoms, $\boldsymbol{D}^{AB}$ ($\boldsymbol{D}^{BA}$), as follows:

$$\boldsymbol{D}^{AB} = \langle\Phi_A(\boldsymbol{k}_c)|\exp\left\{i\left(q\boldsymbol{e}_T\cdot\boldsymbol{R}^{j,m}_{\ell}-\sigma\theta^{\ell}_j\right)\right\}\nabla|\Phi_B(\boldsymbol{k}_v)\rangle, \tag{A5}$$

$$\boldsymbol{D}^{BA} = \langle\Phi_B(\boldsymbol{k}_c)|\exp\left\{i\left(q\boldsymbol{e}_T\cdot\boldsymbol{R}^{j,m}_{\ell}-\sigma\theta^{\ell}_j\right)\right\}\nabla|\Phi_A(\boldsymbol{k}_v)\rangle. \tag{A6}$$

We note that the diagonal matrix elements of the dipole vectors, $\boldsymbol{D}^{AA}$ and $\boldsymbol{D}^{BB}$, vanish because of the symmetry of the p_z wave function, as far as we consider the atomic matrix elements up to the nearest neighbor atoms. Substituting Eq. (3) into Eq. (A5), the dipole vector $\boldsymbol{D}^{BA}$ is calculated as follows:

$$\begin{aligned}\boldsymbol{D}^{BA} &= \frac{1}{N}\frac{1}{U}\sum_{m,m'}\exp\{-i(m'\boldsymbol{k}_c-m\boldsymbol{k}_v)\cdot\boldsymbol{T}\}\\ &\quad\times\sum_{j,j'}\exp\left\{-i\left(\boldsymbol{k}_c\cdot\boldsymbol{R}^{j'}_B-\boldsymbol{k}_v\cdot\boldsymbol{R}^{j}_A\right)\right\}\\ &\quad\times\exp\left\{i\left(q\boldsymbol{e}_T\cdot\boldsymbol{R}^{j,m}_A-\sigma\theta^{A}_j\right)\right\}\\ &\quad\times\left\langle\varphi\left(\boldsymbol{r}-\boldsymbol{R}^{j',m'}_B\right)|\nabla|\varphi\left(\boldsymbol{r}-\boldsymbol{R}^{j,m}_A\right)\right\rangle\\ &\simeq\frac{1}{N}\frac{1}{U}\sum_{m=0}^{U-1}\exp\{-i(\boldsymbol{k}_c-\boldsymbol{k}_v-q\boldsymbol{e}_T)\cdot m\boldsymbol{T}\}\\ &\quad\times\sum_{j=0}^{N-1}\exp\left\{-i(\boldsymbol{k}_c-\boldsymbol{k}_v-q\boldsymbol{e}_T)\cdot\boldsymbol{R}^{j}_A-i\sigma\theta^{A}_j\right\}\\ &\quad\times\sum_{s=1}^{3}\exp\left\{-i\boldsymbol{k}_c\cdot\boldsymbol{r}^{s}_A\right\}\\ &\quad\times\left\langle\varphi\left(\boldsymbol{r}-\boldsymbol{R}^{j,m}_A-\boldsymbol{r}^{s}_A\right)|\nabla|\varphi\left(\boldsymbol{r}-\boldsymbol{R}^{j,m}_A\right)\right\rangle,\end{aligned} \tag{A7}$$

where we set the optical phases $i(q\boldsymbol{e}_T\cdot\boldsymbol{R}^{j,m}_A-\sigma\theta^{A}_j)$ at the carbon atoms of initial states. We note that we consider the matrix element for only the nearest neighbor atoms. Using Eq. (A3), the dipole vector $\boldsymbol{D}^{BA}$ of Eq. (A7) is further calculated as follows:

$$\begin{aligned}\boldsymbol{D}^{BA} &= \frac{1}{N}\frac{1}{U}\sum_{m=0}^{U-1}\exp\{-i(k_c-k_v-q)\cdot mT\}\\ &\quad\times\sum_{j=0}^{N-1}\exp\left\{-i(k_c-k_v-q)\cdot R^{j(z)}_A\right\}\\ &\quad\times\exp\left\{-i(\mu_c-\mu_v+\sigma)\theta^{A}_j\right\}\\ &\quad\times\sum_{s=1}^{3}\exp\left\{-i\boldsymbol{k}_c\cdot\boldsymbol{r}^{s}_A\right\}\left(-\frac{\sqrt{3}m_{\rm opt}}{a}\boldsymbol{r}^{s}_A\right)\\ &=-\frac{\sqrt{3}m_{\rm opt}}{a}\delta(k_c-k_v-q)\delta(\mu_c-\mu_v+\sigma)\boldsymbol{Z}^{*}_A\\ &=\frac{\sqrt{3}m_{\rm opt}}{a}\delta(\boldsymbol{k}_c-\boldsymbol{k}_v+\sigma\boldsymbol{K}_1-\tau\boldsymbol{K}_2)\boldsymbol{Z}_B,\end{aligned} \tag{A8}$$

where $R^{j(z)}_A$ is the z component of $\boldsymbol{R}^{j}_A$ and $\boldsymbol{Z}_A$ ($\boldsymbol{Z}_B$) is defined by

$$\begin{aligned}\boldsymbol{Z}_A &= \sum_{s=1}^{3}\exp\left(i\boldsymbol{k}_c\cdot\boldsymbol{r}^{s}_A\right)\boldsymbol{r}^{s}_A\\ &=-\sum_{s=1}^{3}\exp\left(-i\boldsymbol{k}_c\cdot\boldsymbol{r}^{s}_B\right)\boldsymbol{r}^{s}_B=-\boldsymbol{Z}^{*}_B.\end{aligned} \tag{A9}$$

Here $\boldsymbol{K}_1$, $\boldsymbol{K}_2$, and σ are defined by Eqs. (4) and (7), respectively. The labels μ_v and μ_c denote the cutting lines for valence and conduction bands while k_v and k_c denote the wave numbers on the cutting line [see Eq. (4)]. $\tau=T/\lambda$ is the ratio between the absolute value of translational vector T and the wavelength of the incident light λ. We define

$m_{\rm opt} = \langle\psi(\boldsymbol{r}-\boldsymbol{r}_B^1)|\frac{\partial}{\partial x}|\psi(\boldsymbol{r})\rangle$ [18], using the symmetry of the p_z orbital of carbon atoms in SWNTs. We obtain $\boldsymbol{D}^{AB}$ in the same way as $\boldsymbol{D}^{BA}$, as follows:

$$\boldsymbol{D}^{AB} = \frac{\sqrt{3}m_{\rm opt}}{a}\delta(\boldsymbol{k}_c - \boldsymbol{k}_v + \sigma\boldsymbol{K}_1 - \tau\boldsymbol{K}_2)\boldsymbol{Z}_A, \tag{A10}$$

Using Eqs. (A4), (A8), and (A10), we obtain the formula of the electron-photon matrix element for $\boldsymbol{q} \parallel \boldsymbol{T}$ as follows:

$$M_\sigma^{\parallel}(\boldsymbol{k}_c,\boldsymbol{k}_v) = A\boldsymbol{e}_C\cdot\boldsymbol{C}(\boldsymbol{k}_c,\boldsymbol{k}_v)\delta\big(\boldsymbol{k}_c-\boldsymbol{k}_c^\sigma\big), \tag{A11}$$

where $\boldsymbol{k}_c^\sigma$ and $\boldsymbol{C}(\boldsymbol{k}_c,\boldsymbol{k}_v)$ are, respectively, defined as

$$\boldsymbol{k}_c^\sigma = \boldsymbol{k}_v - \sigma\boldsymbol{K}_1 + \tau\boldsymbol{K}_2. \tag{A12}$$

$$\boldsymbol{C}(\boldsymbol{k}_c,\boldsymbol{k}_v) = \frac{2\sqrt{3}m_{\rm opt}}{a}{\rm Re}\big[C_A^{c*}(\boldsymbol{k}_c)C_B^v(\boldsymbol{k}_v)\boldsymbol{Z}_A\big], \tag{A13}$$

and we use the relationship between the coefficients $\{C_B^{c*}(\boldsymbol{k}_c)C_A^v(\boldsymbol{k}_v)\}^* = -C_A^{c*}(\boldsymbol{k}_c)C_B^v(\boldsymbol{k}_v)$. Noting that $\boldsymbol{k}_c^- = \boldsymbol{k}_v + \boldsymbol{K}_1 + \tau\boldsymbol{K}_2$ for RCP ($\sigma=-1$) and $\boldsymbol{k}_c^+ = \boldsymbol{k}_v + \boldsymbol{K}_1 + \tau\boldsymbol{K}_2$ for LCP ($\sigma=+1$) [see Eqs. (A12)], we can obtain the difference of the intensity of optical absorption between RCP and LCP as follows:

$$\begin{aligned}
&\Delta W_{\rm RL}^{\parallel}(E_L,\boldsymbol{k}_v)\\
&\quad= |M_{-1}^{\parallel}(\boldsymbol{k}_c,\boldsymbol{k}_v)|^2\delta(E_L - E(\boldsymbol{k}_c^-) + E(\boldsymbol{k}_v))\\
&\qquad- |M_{+1}^{\parallel}(\boldsymbol{k}_c,\boldsymbol{k}_v)|^2\delta(E_L - E(\boldsymbol{k}_c^+) + E(\boldsymbol{k}_v))\\
&\quad= |A\boldsymbol{e}_C\cdot\boldsymbol{C}(\boldsymbol{k}_c^-,\boldsymbol{k}_v)|^2\delta(E_L - E_{cv}^-)\\
&\qquad- |A\boldsymbol{e}_C\cdot\boldsymbol{C}(\boldsymbol{k}_c^+,\boldsymbol{k}_v)|^2\delta(E_L - E_{cv}^+),
\end{aligned} \tag{A14}$$

where we define $E_{cv}^\sigma = E(\boldsymbol{k}_c^\sigma) - E(\boldsymbol{k}_v)$. The formula for the CD is given by integrating Eq. (A14) in the first Brillouin zone as follows:

$$\Delta W_{\rm RL}^{\parallel}(E_L) = \sum_{\mu=0}^{N-1}\int_{-\pi/T}^{\pi/T}\Delta W_{\rm RL}^{\parallel}(E_L,\boldsymbol{k}_v)dk_v. \tag{A15}$$

2. Propagation of light perpendicular to nanotube axis

In the case of $\boldsymbol{q} \perp \boldsymbol{T}$, the vector potential of the incident light for either RCP ($\sigma=-1$) or LCP ($\sigma=+1$) that is defined on the unrolled SWNT plane is expressed by [see Fig. 4 and Eq. (18)]

$$\boldsymbol{A}_{\sigma,q}^{\perp}\big(\boldsymbol{R}_\ell^{j,m}\big) = i\sigma A_q^C\big(\boldsymbol{R}_\ell^{j,m}\big)\boldsymbol{e}_C + A_q^T\big(\boldsymbol{R}_\ell^{j,m}\big)\boldsymbol{e}_T, \tag{A16}$$

where the circumference component A_j^C and the amplitude of the axial component A_j^T are, respectively, given by Eqs. (19) and (20),

$$A_q^C\big(\boldsymbol{R}_\ell^{j,m}\big) = A\cos\theta_j^\ell\big(1+i\beta\cos\theta_j^\ell\big), \tag{A17}$$

$$A_q^T\big(\boldsymbol{R}_\ell^{j,m}\big) = A\big(1+i\beta\cos\theta_j^\ell\big), \tag{A18}$$

where $\beta = \pi d_t/\lambda$ is the optical phase for $\boldsymbol{q} \perp \boldsymbol{T}$. The matrix elements of the electron-photon interaction are calculated analytically by putting Eqs. (2), (3), (A18), and (A17) into (A1) as follows:

$$\begin{aligned}
&M_\sigma^{\perp}(\boldsymbol{k}_c,\boldsymbol{k}_v)\\
&\quad= \langle\Psi_c(\boldsymbol{k}_c)|\boldsymbol{A}_{\sigma,q}^{\perp}\big(\boldsymbol{R}_\ell^{j,m}\big)\cdot\nabla|\Psi_v(\boldsymbol{k}_v)\rangle\\
&\quad= A\left(-\sigma\frac{\beta}{2}\boldsymbol{e}_C + \boldsymbol{e}_T\right)\cdot\langle\Psi_c(\boldsymbol{k}_c)|\nabla|\Psi_v(\boldsymbol{k}_v)\rangle\\
&\qquad+ A(i\sigma\boldsymbol{e}_C + i\beta\boldsymbol{e}_T)\cdot\langle\Psi_c(\boldsymbol{k}_c)|\cos\theta_j^\ell\nabla|\Psi_v(\boldsymbol{k}_v)\rangle\\
&\qquad- A\sigma\frac{\beta}{2}\boldsymbol{e}_C\cdot\langle\Psi_c(\boldsymbol{k}_c)|\cos 2\theta_j^\ell\nabla|\Psi_v(\boldsymbol{k}_v)\rangle,
\end{aligned} \tag{A19}$$

Noting $\cos\theta_j^\ell = [\exp(i\theta_j^\ell) + \exp(-i\theta_j^\ell)]/2$, we can calculate each matrix element in Eq. (A19) in the same way with Eq. (A7) and (A8) as follows:

$$\langle\Psi_c(\boldsymbol{k}_c)|\nabla|\Psi_v(\boldsymbol{k}_v)\rangle = \boldsymbol{C}(\boldsymbol{k}_c,\boldsymbol{k}_v)\delta(\boldsymbol{k}_c-\boldsymbol{k}_v), \tag{A20}$$

$$\begin{aligned}
&\langle\Psi_c(\boldsymbol{k}_c)|\cos\theta_j^\ell\nabla|\Psi_v(\boldsymbol{k}_v)\rangle\\
&\quad= \tfrac{1}{2}\boldsymbol{C}(\boldsymbol{k}_c,\boldsymbol{k}_v)\{\delta(\boldsymbol{k}_c-\boldsymbol{k}_v-\boldsymbol{K}_1) + \delta(\boldsymbol{k}_c-\boldsymbol{k}_v+\boldsymbol{K}_1)\},
\end{aligned} \tag{A21}$$

and

$$\begin{aligned}
&\langle\Psi_c(\boldsymbol{k}_c)|\cos 2\theta_j^\ell\nabla|\Psi_v(\boldsymbol{k}_v)\rangle\\
&\quad= \tfrac{1}{2}\boldsymbol{C}(\boldsymbol{k}_c,\boldsymbol{k}_v)\{\delta(\boldsymbol{k}_c-\boldsymbol{k}_v-2\boldsymbol{K}_1) + \delta(\boldsymbol{k}_c-\boldsymbol{k}_v+2\boldsymbol{K}_1)\}.
\end{aligned} \tag{A22}$$

Substituting Eqs. (A20), (A21), and (A22) into (A19), we obtain the matrix element for perpendicular incident light $M_\sigma^\perp(E_L,\boldsymbol{k}_v)$ as follows:

$$\begin{aligned}
M_\sigma^{\perp}(\boldsymbol{k}_c,\boldsymbol{k}_v) &= \langle\Psi_c(\boldsymbol{k}_c)|\boldsymbol{A}_{\sigma,q}^{\perp}\big(\boldsymbol{R}_\ell^{j,m}\big)\cdot\nabla|\Psi_v(\boldsymbol{k}_v)\rangle\\
&= A\left(-\sigma\frac{\beta}{2}\boldsymbol{e}_C + \boldsymbol{e}_T\right)\cdot\boldsymbol{C}(\boldsymbol{k}_c,\boldsymbol{k}_v)\delta(\boldsymbol{k}_c-\boldsymbol{k}_v)\\
&\quad+ A(i\sigma\boldsymbol{e}_C + i\beta\boldsymbol{e}_T)\cdot\frac{1}{2}\boldsymbol{C}(\boldsymbol{k}_c,\boldsymbol{k}_v)\\
&\quad\times\{\delta(\boldsymbol{k}_c-\boldsymbol{k}_v-\boldsymbol{K}_1) + \delta(\boldsymbol{k}_c-\boldsymbol{k}_v+\boldsymbol{K}_1)\}\\
&\quad- A\sigma\frac{\beta}{2}\boldsymbol{e}_C\cdot\frac{1}{2}\boldsymbol{C}(\boldsymbol{k}_c,\boldsymbol{k}_v)\\
&\quad\times\{\delta(\boldsymbol{k}_c-\boldsymbol{k}_v-2\boldsymbol{K}_1) + \delta(\boldsymbol{k}_c-\boldsymbol{k}_v+2\boldsymbol{K}_1)\}.
\end{aligned} \tag{A23}$$

By defining $\boldsymbol{K} = \boldsymbol{k}_c - \boldsymbol{k}_v$, we get Eq. (21). For a given E_L, the difference of optical absorption $\Delta W_{\rm RL}^\perp$ is given by

$$\begin{aligned}
&\Delta W_{\rm RL}^{\perp}(E_L,\boldsymbol{k}_v)\\
&\quad\equiv (|M_{-1}^{\perp}(\boldsymbol{k}_c,\boldsymbol{k}_v)|^2 - |M_{+1}^{\perp}(\boldsymbol{k}_c,\boldsymbol{k}_v)|^2)\delta(E_L - E_{cv})\\
&\quad= A^2\beta[\boldsymbol{e}_C\cdot\boldsymbol{C}(\boldsymbol{k}_c,\boldsymbol{k}_v)][\boldsymbol{e}_T\cdot\boldsymbol{C}(\boldsymbol{k}_c,\boldsymbol{k}_v)]\\
&\qquad\times[2\delta(\boldsymbol{K}) - \delta(\boldsymbol{K}+\boldsymbol{K}_1) - \delta(\boldsymbol{K}-\boldsymbol{K}_1)]\delta(E_L - E_{cv}),
\end{aligned} \tag{A24}$$

where $E_{cv} = E(\boldsymbol{k}_c) - E(\boldsymbol{k}_v)$ is the energy gap between the initial and final states for $\boldsymbol{q} \perp \boldsymbol{T}$.

[1] R. Saito, G. Dresselhaus, and M. S. Dresselhaus, *Physical Properties of Carbon Nanotubes* (Imperial College Press, London, 1998).
[2] R. Saito, M. Fujita, G. Dresselhaus, and M. S. Dresselhaus, Phys. Rev. B **46**, 1804 (1992).
[3] R. Saito, M. Fujita, G. Dresselhaus, and M. S. Dresselhaus, Appl. Phys. Lett. **60**, 2204 (1992).
[4] Ge. G. Samsonidze, A. Grüneis, R. Saito, A. Jorio, A. G. Souza Filho, G. Dresselhaus, and M. S. Dresselhaus, Phys. Rev. B **69**, 205402 (2004).
[5] H. Liu, T. Tanaka, and H. Kataura, Nano Lett. **14**, 6237 (2014).
[6] G. Dukovic, M. Balaz, P. Doak, N. D. Berova, M. Zheng, R. S. Mclean, and L. E. Brus, J. Am. Chem. Soc. **128**, 9004 (2006).
[7] X. Peng, N. Komatsu, S. Bhattacharya, T. Shimawaki, S. Aonuma, T. Kimura, and A. Osuka, Nat. Nanotechnol. **2**, 361 (2007).
[8] F. Wang, K. Matsuda, A. F. M. Mustafizur Rahman, X. Peng, T. Kimura, and N. Komatsu, J. Am. Chem. Soc. **132**, 10876 (2010).
[9] X. Peng, N. Komatsu, T. Kimura, and A. Osuka, ACS Nano **2**, 2045 (2008).
[10] Al. A. Green, M. C. Duch, and M. C. Hersam, Nano Res. **2**, 69 (2009).
[11] X. Wei, T. Tanaka, Y. Yomogida, N. Sato, R. Saito, and H. Kataura, Nat. Commun. **7**, 12899 (2016).
[12] G. Ao, J. K. Streit, J. A. Fagan, and M. Zheng, J. Am. Chem. Soc. **138**, 16677 (2016).
[13] M. Magg, Y. Kadria-Vili, P. Oulevey, R. B. Weisman, and T. Bürgi, J. Phys. Chem. Lett. **7**, 221 (2016).
[14] R. Saito, G. Dresselhaus, and M. S. Dresselhaus, Phys. Rev. B **61**, 2981 (2000).
[15] R. Saito, K. Sato, Y. Oyama, J. Jiang, Ge. G. Samsonidze, G. Dresselhaus, and M. S. Dresselhaus, Phys. Rev. B **72**, 153413 (2005).
[16] A. Sánchez-Castillo, C. E. Román-Velázquez, and C. Noguez, Phys. Rev. B **73**, 045401 (2006).
[17] A. Sánchez-Castillo and C. Noguez, J. Phys. Chem. C **114**, 9640 (2010).
[18] A. Grüneis, R. Saito, Ge. G. Samsonidze, T. Kimura, M. A. Pimenta, A. Jorio, A. G. Souza Filho, G. Dresselhaus, and M. S. Dresselhaus, Phys. Rev. B **67**, 165402 (2003).
[19] Y. Oyama, R. Saito, K. Sato, J. Jiang, Ge. G. Samsonidze, A. Grüneis, Y. Miyauchi, S. Maruyama, A. Jorio, G. Dresselhaus, and M. S. Dresselhaus, Carbon **44**, 873 (2006).
[20] J. Jiang, R. Saito, K. Sato, J. S. Park, Ge. G. Samsonidze, A. Jorio, G. Dresselhaus, and M. S. Dresselhaus, Phys. Rev. B **75**, 035405 (2007).
[21] J. Jiang, R. Saito, Ge. G. Samsonidze, A. Jorio, S. G. Chou, G. Dresselhaus, and M. S. Dresselhaus, Phys. Rev. B **75**, 035407 (2007).
[22] D. P. Craig and T. Thirunamachandran, in *Molecular Quantum Electrodynamics* (Academic, New York, 1984).
[23] Ge. G. Samsonidze, R. Saito, A. Jorio, M. A. Pimenta, A. G. Souza Filho, A. Grüneis, G. Dresselhaus, and M. S. Dresselhaus, J. Nanosci. Nanotechnol. **3**, 431 (2003).
[24] H. Ajiki and T. Ando, Physica B: Condens. Matter **201**, 349 (1994).
[25] S. Uryu and T. Ando, in *Cross-Polarized Exciton Absorption in Semiconducting Carbon Nanotubes*, edited by Ben Murdin and Steve Clowes (Springer Netherlands, Dordrecht, 2008), pp. 119–121.
[26] S. Uryu and T. Ando, Phys. Rev. B **74**, 155411 (2006).
[27] See Supplemental Material at http://link.aps.org/supplemental/10.1103/PhysRevB.95.155436 for the CD of perpendicular and parallel propagation.